Received: 14 October 2022 | Accepted: 18 October 2022

DOI: 10.1002/pamm.202200312

Numerical modelling of stress-strain response and deformation-induced martensite in metastable austenitic stainless steels under monotonic tensile loading

Hari Kisan Thammineni[1,*], **Tong Zhu**[2], **Marek Smaga**[2], **Tilmann Beck**[2], and **Ralf Müller**[1]

[1] Institute for Mechanics, Technical University of Darmstadt, Franzika-Braun-Straße 7, 64287 Darmstadt, Germany
[2] Institute of Materials Science and Engineering, Technical University of Kaiserslautern, Gottlieb-Daimler-Straße, 67663 Kaiserslautern, Germany

A constitutive model describing the deformation-induced martensite transformation in metastable austenitic CrNi steels is presented. In line with the previous work of Stringfellow et al. [1], the material is considered to have a composite response of the underlying austenite and the evolving martensite phases. The stresses and strains in the individual phases are described using viscoplastic models. The effective properties of the material are then computed by a homogenization method. Strain hardening in the individual phases is represented using separate flow rules. Furthermore, based on the plastic strain in the austenitic phase, a transformation kinetics model describes the evolution of the martensite volume, in the two-phase composite.

A numerical implementation of the model is done in the finite element program FEAP [2]. The parameters in model are identified by experimental data using the least-squares optimization. Finally, some results are presented using an illustrative boundary value problem of a structured surface.

1 Introduction

Austenitic stainless steels when alloyed with nickel stabilize the austenitic phase to lower temperatures. The austenite (γ) in these kind of steels is (largely) metastable and requires an external mechanical load to be transformed to a more stable martensitic (α') phase. The kind of mechanical process that drives this phase transformation depends on the temperature. Above martensite start temperature M_s and below a temperature known as M_s^σ, the applied stress assists the transformation in preexisting nucleation sites, by adding the mechanical energy to the existing chemical energy difference between the phases, providing the minimum activation energy required. Above M_s^σ, the stress required for the phase transformation, reaches the yield strength of the material, thus resulting in plastic deformations. This plastic deformation in the austenitic phase results in generation of shear bands, a collective term for active slip systems with ϵ martensite, mechanical twins or grain boundaries, as coined by Olsen and Cohen [3]. The intersections of these shear bands were found to act as potential new martensitic nucleation sites [3, 4]. Thus, this kind of phase transformation process is known as strain or deformation induced transformation, where as the former process is known as stress assisted transformation. The phenomenon of transformation by mechanical loads is observed till a temperature known as M_d, above which the chemical energy difference between the phases is so low that no further phase transformation is possible before fracture [1, 3].

In the current work, the focus is laid on the modelling of deformation induced phase transformation, where the applied deformation drives the transformation of $\gamma \rightarrow \alpha'$. This transformation also results in an inelastic volumetric and deviatoric deformation, a phenomenon known as transformation induced plasticity. This, combined with the strain hardening in the austenite and the evolving martensite phases causes the material to exhibit properties such as high strength and pronounced ductility. The model presented here, is based on the work of Stringfellow et al. [1]. It contains a part that models the stress-strain behavior of composite two phase austenite martensite and another part that models the evolution of phase transformation process.

2 Constitutive model

For the sake of simplicity, a geometric linear strain viscoplastic formulation is used. The corresponding relation for the Cauchy stress $\boldsymbol{\sigma}$ in rate form is given by

$$\dot{\boldsymbol{\sigma}} = \mathbb{C} : (\dot{\boldsymbol{\varepsilon}} - \dot{\boldsymbol{\varepsilon}}^p), \qquad \text{where} \qquad \mathbb{C} = 2G\mathbb{I} + (K - \frac{2}{3}G)\boldsymbol{I} \otimes \boldsymbol{I} \tag{1}$$

represents the isotropic linear elastic modulus. The parameter G is the shear modulus, K is the bulk modulus, $\mathbb{I}$ is the fourth order identity tensor and $\boldsymbol{I}$ is the second order identity tensor. The variables $\dot{\boldsymbol{\varepsilon}}$, $\dot{\boldsymbol{\varepsilon}}^p$ are the total and plastic strain rates

* Corresponding author: e-mail hari.thammineni@tu-darmstadt.de, phone +49 6151 16-22642

respectively. Decomposition of stress and strains in (1) into volumetric and deviatoric components yields,

$$\dot{\boldsymbol{\sigma}} = \dot{\boldsymbol{S}} - \dot{p}\boldsymbol{I} = K(\dot{\varepsilon}_v - \dot{\varepsilon}_v^p)\boldsymbol{I} + 2G(\dot{\boldsymbol{e}} - \dot{\boldsymbol{e}}^p), \tag{2}$$

where p is the pressure or the volumetric stress, $\dot{\varepsilon}_v$ and $\dot{\varepsilon}_v^p$ are the trace of total and plastic strain rates respectively. The deviatoric stress $\boldsymbol{S}$ can be written as a product of an equivalent shear stress τ times the directional tensor $\boldsymbol{N}$ as,

$$\dot{\boldsymbol{S}} = \sqrt{2}\tau\boldsymbol{N}, \qquad \text{where} \qquad \tau = \sqrt{\frac{1}{2}\boldsymbol{S}:\boldsymbol{S}} = \sqrt{\frac{1}{2}}||\boldsymbol{S}||, \qquad \boldsymbol{N} = \frac{\boldsymbol{S}}{||\boldsymbol{S}||}. \tag{3}$$

Similarly, the total and plastic deviatoric strain rates $\dot{\boldsymbol{e}}$ and $\dot{\boldsymbol{e}}^p$ can be written as

$$\dot{\boldsymbol{e}} = \frac{1}{\sqrt{2}}\dot{\gamma}\boldsymbol{M}, \qquad \dot{\boldsymbol{e}}^p = \frac{1}{\sqrt{2}}\dot{\gamma}^p\boldsymbol{N}, \tag{4}$$

where $\dot{\gamma} = \sqrt{2}||\dot{\boldsymbol{e}}||$ and $\dot{\gamma}^p = \sqrt{2}||\dot{\boldsymbol{e}}^p||$ are the total and plastic equivalent shear strains rates respectively. The variable $\boldsymbol{M}$ is a unit tensor coaxial to $\dot{\boldsymbol{e}}$. The strain rate $\dot{\boldsymbol{e}}^p$ is coaxial with the deviatoric stress $\boldsymbol{S}$. Using (3) and (4), relation (2) can be decomposed as

$$\dot{p} = -K(\dot{\varepsilon}_v - \dot{\varepsilon}_v^p), \qquad \dot{\tau} = G(\boldsymbol{M}:\boldsymbol{N}\dot{\gamma} - \dot{\gamma}^p). \tag{5}$$

To compute the rates of p and τ, the evolution equations for $\dot{\varepsilon}_v^p$ and $\dot{\gamma}^p$ are required. The austenitic crystal in its transformation to martensitic crystal structure undergoes an increase in volume and also experiences a change in shape. The rate of increase in volume is captured by $\dot{\varepsilon}_v^p$ and it given as

$$\dot{\varepsilon}_v^p = \Delta_v\dot{f}, \tag{6}$$

where Δ_v represents the relative change in volume associated with $\gamma \rightarrow \alpha'$. The term $\dot{f}$ represents the rate of change of martensite volume fraction f. The change in shape results in a transformation contribution to $\dot{\gamma}^p$, the remaining contributions are due to dislocation movements in the austenitic and the martensitic phases. Thus,

$$\dot{\gamma}^p = A\dot{f} + f\dot{\gamma}_m + (1-f)\dot{\gamma}_a, \tag{7}$$

where the constant A represents the effect of the shape strain orientations on a distribution of nucleation sites. It is computed using the relation,

$$A = A_0 + A_1\left(\frac{\tau}{s_a^*}\right), \tag{8}$$

where s_a^* is the reference stress of austenitic phase, A_0 and A_1 are numerical constants. The evolution of flow stresses in the individual phases $\dot{\gamma}_{a/m}$ is defined using a viscoplastic model with a power-law relation as,

$$\dot{\gamma}_{a/m} = \dot{\gamma}_0^*\left(\frac{\tau_{a/m}}{s_{a/m}}\right)^M, \tag{9}$$

where $\dot{\gamma}_0^*$ is a reference strain rate, $M \geq 1$ is a material constant and $s_{a/m}$ represent the current shear strength of the austenitic and martensitic phases respectively. The relation between global and the local stresses and strain rates in the individual phases can be given by the use of homogenization methods. Here, in order to avoid the computational cost due to iterative solving of nonlinear homogenization equations at the material level, as it is in the case of Stringfellow et al. [1], a simple Sachs/Reuss homogenization scheme is used. This scheme assumes that the stress, both in local and global domains, are identical, thus resulting in $\tau = \tau_a = \tau_m$. Under this assumption, (9) becomes

$$\dot{\gamma}_{a/m} = \dot{\gamma}_0^*\left(\frac{\tau}{s_{a/m}}\right)^M. \tag{10}$$

The shear strength of the austenitic and martensitic phases $s_{a/m}$ increases due to the strain hardening caused by the plastic deformation. Martensite, being lot harder that austenite, has significantly different hardening behavior in comparison to the austenite. So, two separate hardening laws are used

$$s_{a/m} = s_{a/m}^*\left(1 + \frac{\gamma_{a/m}}{\gamma_{a/m}^*}\right)^{n_{a/m}}. \tag{11}$$

3 Phase transformation kinetics

A numerical model for the deformation induced $\gamma \rightarrow \alpha'$ was initially proposed by Olsen and Cohen [3]. Considering the shear band intersections as potential martensitic nucleation points, they proposed a 1D model that depends on temperature and the plastic strain rate in austenite. Stringfellow et al. [1] generalized this model to 3D, coupled it with the stress strain response and also considered the influence of stress state on the phase transformation. The evolution model used in the present work is adapted from Stringfellow et al. [1] and the presentation style below is followed from Papatriantafillou et al. [5].
The rate of change of the martensitic volume fraction f is given by

$$\dot{f} = (1-f)(A_f \dot{\gamma}_a + B_f \dot{\Sigma}), \tag{12}$$

where as Σ is stress triaxiality and is defined in (13). The factor $(1-f)$ forces the rate of phase transformation to decrease with the consumption of available austenite volume, resulting in sigmoidal transformation curves.

$$\Sigma = -\frac{p}{\sqrt{3}\tau} \tag{13}$$

The coefficient A_f is given by

$$A_f = \alpha\beta r(1-f_{sb})(f_{sb})^{(r-1)}P, \tag{14}$$

where f_{sb} is the volume fraction of shear bands in austenite. It evolves with the plastic strain

$$\dot{f}_{sb} = (1-f_{sb})\alpha\dot{\gamma}_a, \tag{15}$$

where α is a constant representing the rate of shear band formation $df_{sb}/d\gamma_a$. Its value decreases with an increase in temperature. The parameter r is the exponent that models the randomness of shear band orientations and β is a geometrical constant. Based on the observation that martensite grows only in a certain fraction of shear band intersections that cross the minimum thermodynamic energy barrier, a probability parameter P is defined. It is cast in the form of Gaussian cumulative probability distribution of the normalized thermodynamic driving force g.

$$P = \frac{1}{\sqrt{2\pi}S_g}\int_{-\infty}^{g} \exp\left[-\frac{1}{2}\left(\frac{g'-\bar{g}}{s_g}\right)^2\right]dg', \tag{16}$$

where $\bar{g}$ and s_g are the mean and the standard deviation of the distribution of the minimum g values required for the activation of shear band intersections. The driving force g considers the influences of temperature and stress by the relation

$$g = g_0 + g_1\Theta + g_2\Sigma, \tag{17}$$

where g_0, g_1, g_2 are dimensionless constants, Θ is the normalized temperature related to the absolute temperature T by

$$\Theta = \frac{T - M_s^\sigma}{M_d - M_s^\sigma}. \tag{18}$$

The coefficient B_f is given by the expression

$$B_f = \beta {f_{sb}}^r \frac{g_2}{\sqrt{2\pi}S_g}\exp\left[-\frac{1}{2}\left(\frac{g-\bar{g}}{S_g}\right)^2\right]H(\dot{\Sigma}), \tag{19}$$

where $H(\dot{\Sigma})$ is the Heaviside function of the stress triaxiality rate.

4 Numerical implementation

The model is implemented as a material routine in a finite element environment. The time differential equations shown above are integrated using explicit integration at the material level, where as the global finite element formulations are integrated implicitly and are solved using Newton's method. A general overview of the steps involved in solving the material equations is presented below.

The simulation is considered to be displacement driven. Thus for a given time increment $[t_n, t_{n+1}]$ and at a given Gauss point, the values of strain $\boldsymbol{\varepsilon}_{n+1}$ and the strain rate $\dot{\boldsymbol{\varepsilon}}$ at the time t_{n+1} are known. Also known are the values of stress $\boldsymbol{\sigma}_n$ and the internal variables $(f_n, \gamma_a|_n, \gamma_m|_n, \dot{p}, \dot{\tau})$ at time t_n, the updated values of these variables have to be evaluated at the time t_{n+1}. The steps for the corresponding computation are as follows:

Using $\boldsymbol{\sigma}_n$, the pressure p and the deviatoric stress $\boldsymbol{S}$ at time t_n are computed by

$$p_n = -\frac{\sigma_{ii}|_n}{3}, \qquad \boldsymbol{S}_n = \boldsymbol{\sigma}_n + p_n \boldsymbol{I}. \tag{20}$$

With these results, the values of τ_n, Σ_n can be computed using (3) and (13). Furthermore, the value of $\dot{\Sigma}$ can be calculated using the relation given in Stringfellow et al. [1] as

$$\dot{\Sigma} = \Sigma\left(\frac{\dot{p}}{p_n} - \frac{\dot{\tau}}{\tau_n}\right). \tag{21}$$

In the next step, $\dot{\boldsymbol{\varepsilon}}$ is decomposed into volumetric $\dot{e}_v$ and deviatoric $\dot{\boldsymbol{e}}$ components. Then the equivalent strain rate $\dot{\gamma}$ and the directional tensor $\boldsymbol{M}$ of $\dot{\boldsymbol{e}}$ are computed. In the following step, the trail deviatoric stress $\boldsymbol{S}^{tr}$ is computed by

$$\boldsymbol{S}^{tr} = \boldsymbol{S}_n + 2G\dot{\boldsymbol{e}}\Delta t, \tag{22}$$

where, $\Delta t = t_{n+1} - t_n$. The unit tensor $\boldsymbol{N}$ can be obtained from

$$\boldsymbol{N} = \frac{\boldsymbol{S}^{tr}}{||\boldsymbol{S}^{tr}||}. \tag{23}$$

Thereafter, using the values of $\gamma_a|_n$, $\gamma_m|_n$ and τ_n the shear strengths $s_{a/m}|_n$ and the rate of increase of plastic strains $\dot{\gamma}_{a/m}$ in the individual phases are computed using the relations (11) and (10). The shear band volume fraction f_{sb} at time t_n is computed in the next step, using a relation obtained from the integration of (15) as

$$f_{sb}|_n = 1 - e^{-\alpha\gamma_a|_n}. \tag{24}$$

In the following step, the values of driving force g and the cumulative probability P are calculated at time t_n, using (17) and (16). With the results above, the coefficients A_f and B_f at time t_n are evaluated:

$$A_f|_n = \alpha\beta r(1 - f_{sb}|_n)(f_{sb}|_n)^{(r-1)}P_n, \qquad B_f|_n = \beta {f_{sb}|_n}^r \frac{g_2}{\sqrt{2\pi}S_g} \exp\left[-\frac{1}{2}\left(\frac{g_n - \bar{g}}{S_g}\right)^2\right] H(\dot{\Sigma}). \tag{25}$$

The rate of martensite volume fraction $\dot{f}$ can be obtained from

$$\dot{f} = (1 - f_n)(A_f|_n\,\dot{\gamma}_a + B_f|_n\,\dot{\Sigma}). \tag{26}$$

In the following step, the equivalent volumetric and the deviatoric plastic strain rates $\dot{e}_v^p, \dot{\gamma}^p$ of the material are derived from

$$\dot{e}_v^p = \Delta v \dot{f}, \qquad \dot{\gamma}^p = A_n\dot{f} + f_n\dot{\gamma}_m + (1 - f_n)\dot{\gamma}_a. \tag{27}$$

Using these strain rates, the corresponding equivalent stress rates $\dot{p}$ and $\dot{\tau}$ are computed as

$$\dot{p} = -K(\dot{e}_v - \dot{e}_v^p), \qquad \dot{\tau} = G(\boldsymbol{M} : \boldsymbol{N}\dot{\gamma} - \dot{\gamma}^p). \tag{28}$$

The next step involves updating the internal variables to time t_{n+1} using an explicit integration scheme:

$$\begin{aligned}
f_{n+1} &= f_n + \dot{f}\Delta t,\\
\gamma_a|_{n+1} &= \gamma_a|_n + \dot{\gamma}_a\Delta t,\\
\gamma_m|_{n+1} &= \gamma_m|_n + \dot{\gamma}_m\Delta t,\\
p_{n+1} &= p_n + \dot{p}\Delta t,\\
\tau_{n+1} &= \tau_n + \dot{\tau}\Delta t.
\end{aligned} \tag{29}$$

Finally, using the updated equivalent stresses p_{n+1}, τ_{n+1}, the stress tensor at time t_{n+1} is available from

$$\begin{aligned}
\boldsymbol{S}_{n+1} &= \sqrt{2}\tau_{n+1}\boldsymbol{N},\\
\boldsymbol{\sigma}_{n+1} &= \boldsymbol{S}_{n+1} - p_{n+1}\boldsymbol{I}.
\end{aligned} \tag{30}$$

This concludes the integration process for the current time increment $[t_n, t_{n+1}]$ and the steps are repeated for the subsequent increments. For solving the global FE formulations using the Newton's method, a material tangent ${}^{\Delta\boldsymbol{\sigma}_{n+1}}/_{\Delta\boldsymbol{\varepsilon}_{n+1}}$ has to be provided. This tangent, updated at every time increment (usually) results in fast convergence. In the current work, the material tangent at all time increments is considered to be same as the isotropic elastic tensor $\mathbb{C}$, shown in (1). This assumption, may result in more iterations for the convergence, but it won't have any influence on the final converged result.

5 Parameter identification

The parameters in the current material model have to be estimated, so that the model is able to replicate the experimental behavior of the considered metastable austenitic steel AISI 347. The values of elasticity modulus E, Poisson's ratio ν of the considered material and the values of the parameters that are adapted directly from Stringfellow et al. [1], are shown in the Table 1.

Table 1: Material constants of AISI 347 and parameters adapted from previous works.

E	ν	r	$\bar{g}$	s_g	g_1	g_2	$\dot{\gamma}_0^*$	M	A_0	A_1	Δv
191 GPa	0.27	4	3220	290	1450	490	0.007	40	0.02	0.02	0.03

Since the experimental determination of M_s^σ and M_d temperatures is difficult, the value of M_s^σ is taken to be same as M_s temperature ($192.018K$ for AISI 347 [6]) and the value of M_d is assumed to be $400K$. Further, an attempt has been made to estimate the parameters $(s_a^*, \gamma_a^*, n_a, s_m^*, \gamma_m^*, n_m)$ that model the hardening behavior of the individual austenitic and martensitic phases, by fitting the corresponding hardening laws given in (11) with the experimental data of uniaxial tensile tests. For the estimation of the hardening parameters of austenite, the plastic flow data of stable austenitic steel AISI 904L is used and for the case of martensite, the parameters are fitted to a flow curve of a pre-worked AISI 347 steel with 80% final martensite content. The corresponding plots are shown in Fig. 1 and 2, the resulted hardening parameter values are shown in Table 2.

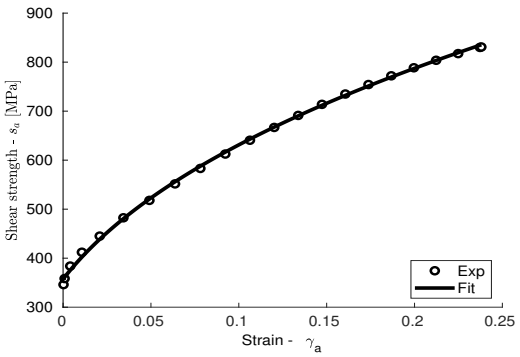

Fig. 1: Fit of austenitic hardening law with AISI 904L.

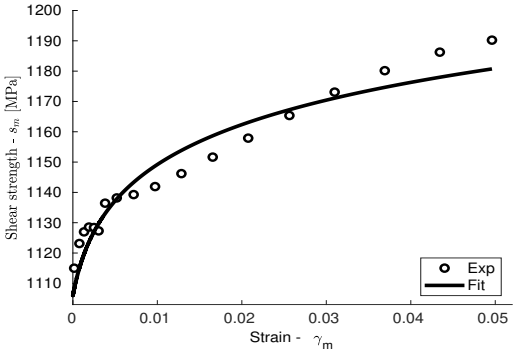

Fig. 2: Fit of martensitic hardening law with 80% martensite AISI 347.

Table 2: Fitted hardening parameters of austenite and martensite phases.

s_a^*	γ_a^*	n_a	s_m^*	γ_m^*	n_m
357 MPa	0.0299	0.3872	1106 MPa	0.0014	0.018

It can be seen that in case of martensite, the fit shown in Fig. 2 is not optimal. Using these parameters, the remaining parameters were estimated by fitting them simultaneously with the experimental stress-strain and the martensite evolution curves obtained during the uniaxial tensile loading of AISI 347 at a temperature of 192 K [6]. For this, the model is implemented in finite element analysis program FEAP [2], using 8-noded solid elements and bi-linear shape functions. A two objective least square error function, one for the stress-strain data and one for the martensite evolution-strain data are weighted to compute the total error. This constrained optimization problem was then solved using the inbuilt MATLAB algorithm fmincon.

This identification approach of fixing the parameters shown in Tables 1, 2 and trying to estimate the remaining parameters, led to non-conclusive results. The reason for this as mentioned in [7], could be that the hardening behavior estimated in the Table 2, may not be able to correctly model the flow behavior of the individual phases that evolve with the plastic deformation. After some trail and error, one of the combination that gave conclusive results is obtained by fixing the hardening parameters of martensite along with the others mentioned in Table 1 and let the austenite hardening parameters be estimated along with the remaining ones. The results is shown in the Fig. 3, 4 and the estimated parameters are given in the Table 3.

Table 3: Fitted remaining material parameters.

α	β	s_a^*	γ_a^*	n_a	g_0
4.16	1.88	129MPa	0.0053	0.2008	3624

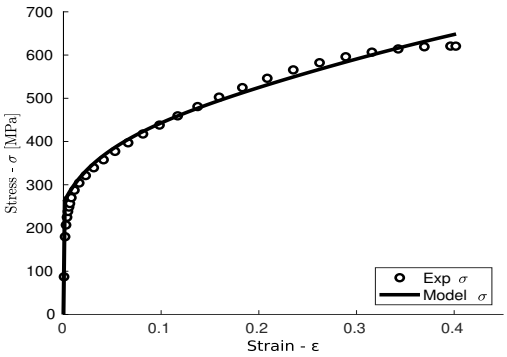

Fig. 3: Fit with stress-strain data of AISI 347.

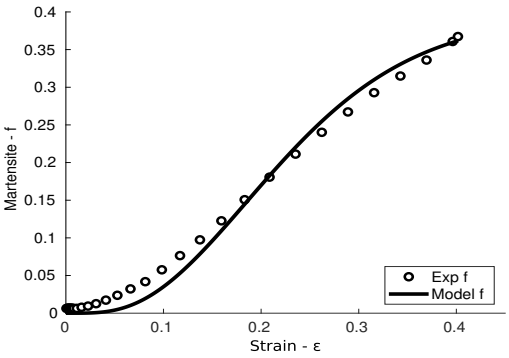

Fig. 4: Fit with martesnite evolution-strain data of AISI 347.

6 Results

The application of the model is demonstrated by an illustrative boundary value problem of structured surface, as shown in Fig. 5. Boundary conditions prevent it from moving vertically. Also the deformations in thickness direction are restricted. The body is displaced horizontally, up to a strain of 5%, in a duration of 100 s. Before deformation the material is considered to be in 100% austenitic phase. The corresponding results of the stress in the horizontal direction and the martensite evolution due to the applied deformation, are shown in Fig. 6 and 7.

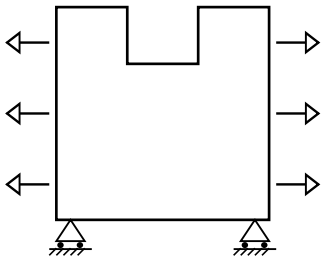

Fig. 5: Boundary value problem with structured surface.

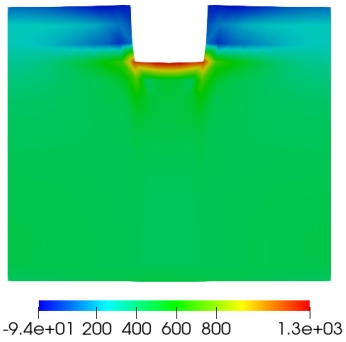

Fig. 6: Stress distribution in horizontal direction.

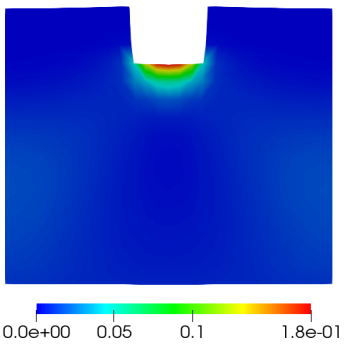

Fig. 7: Martensite evolution f.

The bottom of the grove, experiences higher stresses due to the geometry, thus a visible phase transformation is to be observed. There, as it can be seen in Fig. 7, around 18 % of austenite has transformed to martensite.

Acknowledgements Funded by the Deutsche Forschungsgemeinschaft (DFG, German Research Foundation) - Projektnummer 172116086 - SFB 926. Open access funding enabled and organized by Projekt DEAL.

References

[1] R. G. Stringfellow, D. M. Parks and G. B. Olson, Acta metallurgica et materialia **40(7)**, 1703-1716 (1992).
[2] Programming - FEAP Wiki, http://feap.berkeley.edu/wiki/index.php/Programming, Accessed: 2022-10-08.
[3] G. B. Olson, and M. Cohen, Metallurgical transactions A **6(4)**, 791 (1975).
[4] G. B. Olson, and M. Cohen, J. LessCommon Met **28(1)** 107-118 (1972).
[5] I. Papatriantafillou, N. Aravas and G. N. Haidemenopoulos, Steel research international **75(11)**, 730-736 (2004).
[6] M. Smaga, R. Skorupski, D. Eifler and T.Beck, Journal of Materials Research **32**, 4452-4460 (2017).
[7] S. Prüger, M. Kuna, S. Wolf and L. Krügerm, Steel research international **82(9)**, 1070-1079 (2011).

